International Journal of Offshore and Polar Engineering (ISSN 1053-5381)

Vol. 31, No. 1, March 2021, pp. 1–10; https://doi.org/10.17736/ijope.2021.jc820

http://www.isope.org/publications

A Comparative Study on the Nonlinear Interaction Between a Focusing Wave and Cylinder Using State-of-the-art Solvers: Part A

V. Sriram[1], Shagun Agarwal[1], Shiqiang Yan*[2], Zhihua Xie*[3], Shaswat Saincher[1], Torsten Schlurmann[4], Qingwei Ma*[2], Thorsten Stoesser[5], Yuan Zhuang[6], Bo Han[6], Weiwen Zhao*[6], Xiaotong Yang[6], Z. Li[6], Decheng Wan*[6], Yi Zhang[7], Bin Teng*[7], Dezhi Ning*[7], Ningbo Zhang[8], Xing Zheng*[8], Guochun Xu[9], Jiaye Gong*[10], Yunbo Li[10], Kangping Liao[8], Wenyang Duan[8], Ronggui Han[11], Windiman Asnim[2], Zana Sulaiman[12], Zhongbing Zhou[7], Jianmin Qin[7], Yucheng Li[7], Zhiwei Song[7], Xiaofan Lou[7], Lin Lu*[7], Changfu Yuan[7], Yuxiang Ma*[7], Congfang Ai[7], Guohai Dong[7], Hanbing Sun[8], Qiang Wang[8], Zhi-Tao Zhai[8], Yan-Lin Shao[13], Zaibin Lin[14], Ling Qian*[14], Wei Bai[14], Zhihua Ma*[14], Pablo Higuera[15], Eugeny Buldakov[5], Dimitris Stagonas[16,22], Santiago Martelo Lopez[3], Aristos Christou*[5], Pengzhi Lin[17], Yanyan Li*[18], Jinshu Lu*[18], Sa Young Hong*[19], Yoon-Jin Ha[19], Kyong-Hwan Kim*[19], Seok-Kyu Cho[19], Dong-Min Park[19], Wojciech Laskowski[13], Claes Eskilsson[20], Mario Ricchiuto[21], Allan P. Engsig-Karup[13], Lin Cheng[23], Jinhai Zheng[23], Hanbin Gu*[9], Guangnian Li[9]

[1]Indian Institute of Technology Madras, India; [2]City, University of London, UK; [3]Cardiff University, UK; [4]Leibniz University of Hannover, Germany; [5]University College London, UK; [6]Shanghai Jiao Tong University, China; [7]Dalian University of Technology, China; [8]Harbin Engineering University, China; [9]Ningbo University, China; [10]Shanghai Maritime University, China; [11]Yantai CIMC Raffles Offshore Limited, China; [12]GustoMSC B.V., The Netherlands; [13]Technical University of Denmark, Denmark; [14]Manchester Metropolitan University, UK; [15]University of Auckland, New Zealand; [16]Cranfield University, UK; [17]Sichuan University, China; [18]Zhejiang Ocean University, China; [19]Korea Research Institute of Ships and Ocean Engineering, Korea; [20]Research Institutes of Sweden, Sweden; [21]Inria Bordeaux–Sud-Ouest, France; [22]University of Cyprus, Cyprus; [23]Hohai University, China

This paper presents ISOPE's 2020 comparative study on the interaction between focused waves and a fixed cylinder. The paper discusses the qualitative and quantitative comparisons between 20 different numerical solvers from various universities across the world for a fixed cylinder. The moving cylinder cases are reported in a companion paper as part B (Agarwal, Saincher, et al., 2021). The numerical solvers presented in this paper are the recent state of the art in the field, mostly developed in-house by various academic institutes. The majority of the participants used hybrid modeling (i.e., a combination of potential flow and Navier–Stokes solvers). The qualitative comparisons based on the wave probe and pressure probe time histories and spectral components between laminar, turbulent, and potential flow solvers are presented in this paper. Furthermore, the quantitative error analyses based on the overall relative error in peak and phase shifts in the wave probe and pressure probe of all the 20 different solvers are reported. The quantitative errors with respect to different spectral component energy levels (i.e., in primary, sub-, and superharmonic regions) capturing capability are reported. Thus, the paper discusses the maximum, minimum, and median relative errors present in recent solvers as regards application to industrial problems rather than attempting to find the best solver. Furthermore, recommendations are drawn based on the analysis.

INTRODUCTION

Recently, several numerical codes have been made available as open-source or commercial packages, and some have been developed in academia. These are based on a variety of underlying mathematical models encompassing both new and traditional computational methods, yet there still remains considerable uncertainty in their application and reliability. Many attempts have been made by researchers to collaborate and validate their in-house-developed codes. (See Clément, 1999; Loysel et al., 2012; Ransley et al., 2019, 2020; and Tanizawa and Clément, 2000.) The performance of these solvers is problem dependent. Although a given solver may prove to be the best choice for some applications, it may not perform well for other applications. Hence, these solvers need to be tested for a sufficiently wide range of applications.

In the present study, the laboratory measurements on focusing wave interactions with a fixed cylinder and a moving cylinder have been released for participants to compare with their numerical model. The objective of this comparative study is to (a) understand how well the recent state-of-the-art numerical solvers perform and what type of solvers the participants prefer for this application; (b) instead of finding a best solver, rather estimate overall maximum, minimum, and median errors that are present in these recent codes; (c) assess the overall performance of these solvers in capturing the primary, superharmonic, and subharmonic components, as well as the relative error in pressure and wave probe time history; and (d) evaluate the overall performance in simulating small-amplitude and large-amplitude focusing waves. Finally, a reasonable quantification of the "acceptable error" is provided to the numerical modeling community/users/developers as a guideline for future investigations; this is something that is

*ISOPE Member.

Received September 23, 2020; revised manuscript received by the editors January 5, 2021. The original version was submitted directly to the Journal.

KEY WORDS: Comparative study, hybrid modeling, Navier–Stokes, potential flow, fixed cylinder, moving cylinder, validation.

Case	f_c (Hz)	$\delta f/f_c$	f_1 (Hz)	t_f (s)	N	G_a
1	0.68	1.00	0.34	38.0	32	0.001
3	0.68	1.00	0.34	38.0	32	0.003

Note: f_c, center frequency; Δf, frequency bandwidth; t_f, focusing time; N, number of wave packets; G_a, amplitude gain parameter.

Table 1 Tested wave packet characteristics

currently not available, to the best of our knowledge. The present paper is an attempt toward meeting these objectives. The present paper deals with the fixed cylinder comparative study results; the moving cylinder results are reported in Agarwal, Saincher, et al. (2021).

EXPERIMENTAL DETAILS

The experiments were performed using the wave tank in the Ludwig Franzius Institute at Leibniz University of Hannover, Germany. The experimental results that are used in this paper correspond to the wave characteristics, as shown in Table 1, generated based on the second-order wavemaker theory. There are seven wave probes and eight pressure transducers deployed to measure the focusing wave evolution and pressures on the cylinder. The details are relegated to Sriram et al. (2021), along with the experimental error analysis in this journal volume, so they shall not be repeated here for the sake of brevity. The constant steepness spectrum has been adopted. The choice of a constant steepness for studying nonlinearity as opposed to a constant amplitude is prudent, because the effects of nonlinearity on the evolution of the focusing wave group will be uniform across the spectral components, owing to a single value of steepness across the spectrum. Thus, the numerical model capability can be accessed, as the focusing is sensitive to the capture of the manifestation of the sub- and superharmonic components and its spectral evolution correctly.

PARTICIPATING CODES AND DATA PROCESSING

The list of participating universities, the code names/labels used in the present paper, and the code details are presented in Table 2. There are 20 different codes, each of which differs in terms of the numerical schemes, methodology, and physics involved. An interesting observation from this table is that most of the participants used hybrid modeling; that is, in the far field, the potential flow theory (referred in Table 2 as P) is used, and near the cylinder, they have used Navier–Stokes (NS) equations, in either the laminar (NSL) or turbulent frameworks (NST). In hybrid modeling, most of the participants have adopted a weakly coupled approach (or one-way coupling), which is sufficient for the present transient focused wave simulation. The methods involved are finite volume (FVM), finite element (mostly for potential flow), finite difference, and particle methods (SPH and MLPGR). Almost all the codes are developed in-house in OpenFOAM with a sole exception being the commercial software STAR-CCM+ employed in a couple of studies. More details about the code methodology and other aspects can be referred in the citations therein or in this volume of the journal. The simulation data from the participants are obtained at a sampling frequency of 100 Hz for both wave and pressure probe readings at the mentioned locations (see Sriram et al., 2021). Furthermore, the participants were instructed to provide the data with respect to wave probe 1 (WP1) (i.e., incident wave probe at $x = +4.98$ m), in order to understand the phase shift between the numerical codes. No filtering or noise removal

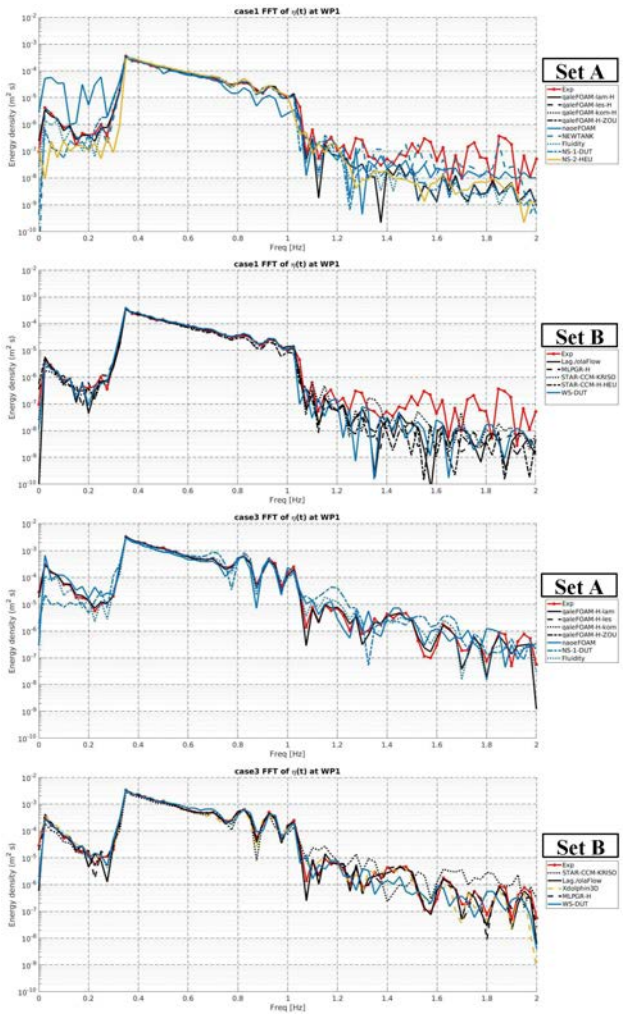

Fig. 1 Comparison of spectral energy distribution for surface elevation $\eta(t)$ signals recorded near the wave paddle at WP1 ($x = +4.98$ m)

was carried out during the comparison process. Furthermore, some participants did not report some wave probe or pressure probe results.

RESULTS AND DISCUSSION

Fidelity of Wave-packet Generation

The submitted results were first evaluated based on how accurately the numerical wavemaker input (either piston-type or a Dirichlet input from the spectrum) develops into wave packets that would undergo focusing near the cylinder. The majority of the participants used a piston-type wavemaker, except five codes, wherein Dirichlet-type boundary conditions were used. The participating studies have been grouped into two sets, A and B, to facilitate readability of the plots. Note that this segregation is not based on any criteria.

This shows the advances in implementing the moving boundary in the present modeling technology, which was challenging a decade ago. To evaluate the performance, we restricted to a frequency domain analysis, as the comparison of the input energy at different packet frequencies is of interest. To assess the fidelity of wave packet generation, fast Fourier transform (FFT) analysis of the free-surface elevation $\eta(t)$ signals recorded by the WP1 gauge close to the wavemaker was carried out. The results from

the comparative analysis are presented in Fig. 1. It may be inferred from Fig. 1 that the general agreement between the simulations and experimental FFT plots is good. In the case of the steeper wave (case 3), the simulations are seen to successfully capture the energy content within the primary range ($f \in [0.34 : 1.02$ Hz]) as well as for the sub- ($0 < f < 0.34$ Hz) and superharmonics ($1.02 < f < 2.04$ Hz). However, it is also seen from Fig. 1 that a general difficulty exists in capturing the superharmonic wave packets for the smaller focused wave (case 1), which seems to be independent of the numerical framework chosen for simulation. The said difficulty may be attributed to the small amplitude of these packets, which makes it challenging to capture them in a simulation, and numerical damping is inevitable if mesh convergence is not sufficiently established. Thus, from this study it can be concluded that the capturing of small-amplitude focusing is challenging when compared with large-amplitude waves, irrespective of the wave generation method employed.

Fidelity of Wave Focusing

Next, the submitted results are evaluated in terms of the fidelity/closeness with which the simulations resemble the experiments in replicating the wave-focusing event in front of the cylinder, after propagation to a distance of 24.31 m. The qualitative assessment is done in terms of comparing the profile of the focused wave generated just in front of the cylinder (WP5) as well as the energy contents of its constituent harmonics. The time domain assessment of $\eta(t)$ signals recorded at WP5 for cases 1 and 3 is presented at the top of Figs. 2 and 3, respectively. It can be observed that most of the solvers correctly replicate the focused wave profile, with numerical damping only observed in a couple of cases. It is interesting to note that, for the same wave input, a considerable scatter occurs in the wave phase at the focusing point; this is especially true for the smaller wave, case 1. This may be attributed to the noncapturing of the higher harmonics at WP1, eventually leading to a phase shift across various solvers. However, given the fact that the participants were at liberty to choose the numerical framework for simulation, the submissions are not judged based on phase agreement but rather in terms of the energy contents captured during focusing. The spectral energy density spectra corresponding to the $\eta(t)$ signals recorded at WP5 for cases 1 and 3 are presented at the bottom of Figs. 2 and 3, respectively. Barring a couple of solvers, almost all models are accurate in predicting the spectral energy within the subharmonic and primary frequency bands ($f \leq 1.02$ Hz). However, a large discrepancy is observed between the simulations and experiments as well as amongst the different models in capturing the energy contents of the superharmonics; this is especially noticeable for case 3.

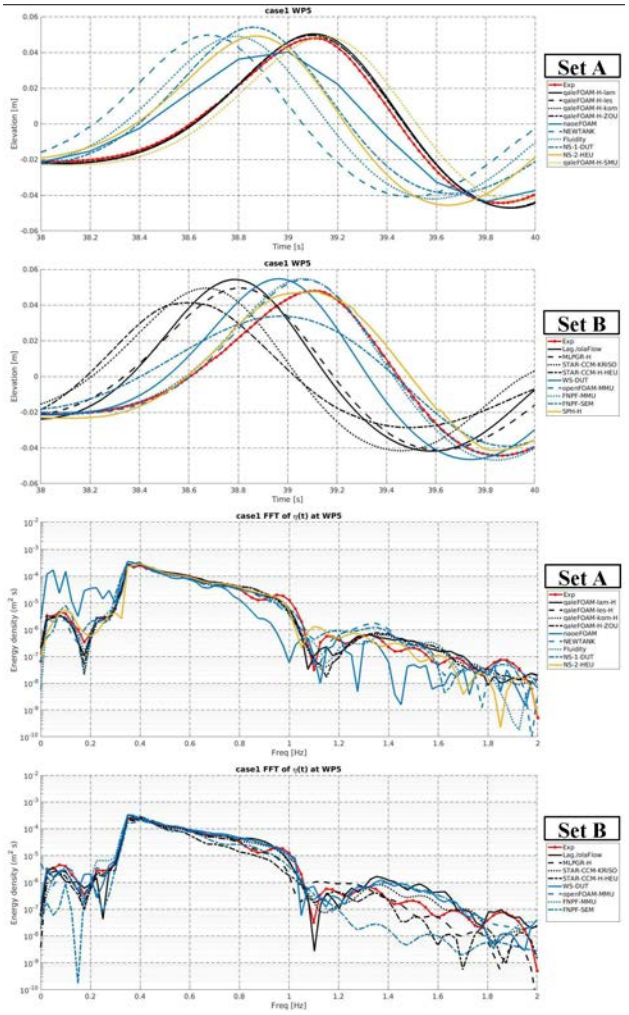

Fig. 2 Comparison of time series and spectral energy distribution for $\eta(t)$ signals recorded in front of the cylinder at WP5 ($x = +24.31$ m) for the smaller wave (case 1)

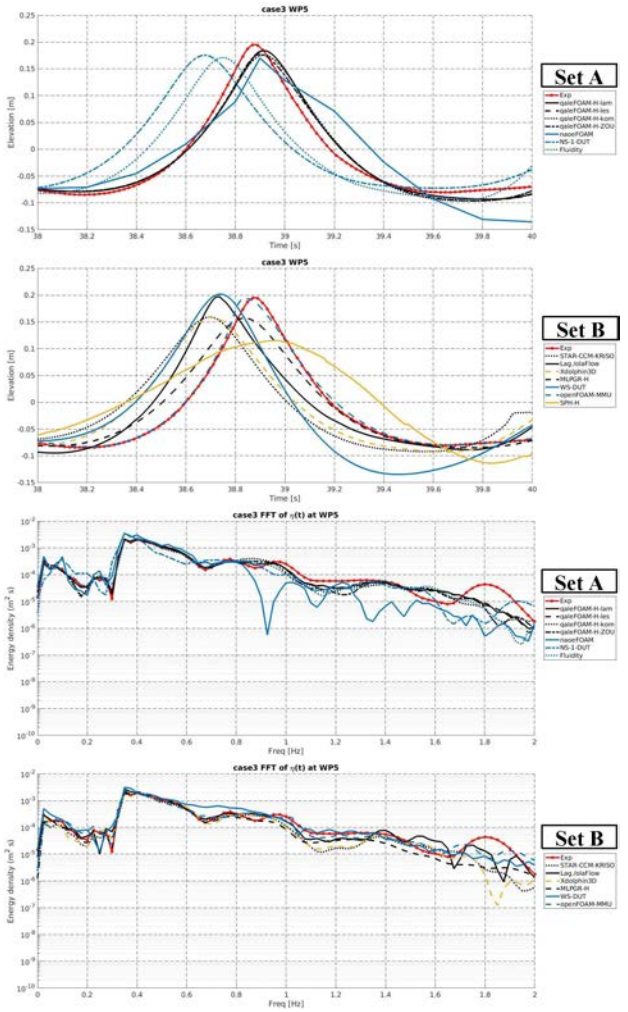

Fig. 3 Comparison of time series and spectral energy distribution for $\eta(t)$ signals recorded in front of the cylinder at WP5 ($x = +24.31$ m) for the larger wave (case 3)

S/N	Name of the participating university	Code name/label	P/ NSL/ NST	Method	Turbulence scheme	1-phase / 2-phase	Wavemaker or source function	L_{NS}(m)	$D/\Delta x$	IH/ OS/C
1	Indian Institute of Technology Madras (Agarwal, Sriram, et al., 2021)	IITM MLPGR-H	P-NSL	FEM-MLPGR	—	1-phase	Piston-WC	4	6	IH
2	City, University of London (Li et al., 2018; Yan et al., 2020)	qaleFOAM-H-lam	P-NSL	FEM-FVM	—	2-phase	Piston-WC	2.2	15	IH/ OS
3	City, University of London (Li et al., 2018; Yan et al., 2020)	qaleFOAM-H-LES	P-NST	FEM-FVM	Large-Eddy Simulation (LES)	2-phase	Piston-WC	2.2	61	IH/ OS
4	City, University of London (Li et al., 2018; Yan et al., 2020)	qaleFOAM-H-kom	P-NST	FEM-FVM	k-ω SST (Shear Stress Transport)	2-phase	Piston-WC	2.2	22	IH/ OS
5	Shanghai Maritime University (Li et al., 2018; Yan et al., 2020)	qaleFOAM-H-SMU	P-NST	FEM-FVM	k-ω SST	2-phase	Piston-WC	2.2	550	IH/ OS
6	Cardiff University (Xie and Stoesser, 2020)	Xdolphin3D	NST	FVM	LES	2-phase	Piston	N/A	11	IH
7	Shanghai Jiao Tong University (Shen and Wan, 2016)	naoe-FOAM-SJTU	NSL	FVM	—	2-phase	Piston	N/A	17	IH/ OS
8	Dalian University of Technology (Zhang and Teng, 2019; Zhang et al., 2020)	WS-DUT	P	HOBEM	—	1-phase	Dirichlet	N/A	44	IH
9	Dalian University of Technology (Xie et al., 2017)	Fluidity	NSL	FEM	Direct Numerical Simulation (DNS)	1-phase	Piston	N/A	1,100	OS
10	University of Auckland & University College London (Buldakov et al., 2019; Higuera, 2020)	Lag./olaFlow	P-NST	FDM-FVM	k-ω SST	2-phase	Piston-WC	1.77	147	IH/ OS
11	Dalian University of Technology (Ai et al., 2011, 2019; Ma et al., 2019)	NS-1-DUT	P or NST	FVM	LES	1-phase	Dirichlet	N/A	N/A	IH
12	Zhajiang Ocean University (Li et al., 2018; Gong et al., 2020; Yan et al., 2020)	qaleFOAM-H-ZOU	P-NSL	FEM-FVM	—	2-phase	Piston-WC	4	88	IH/ OS
13	Harbin Engineering University (Wang et al., 2020)	STAR CCM-H-HEU	P-NST	FVM	Realizable k-ε	2-phase	Piston-WC	N/A	55	C
14	Harbin Engineering University (Liao and Hu, 2013; Liao et al., 2017)	NS-2-HEU	NST	FDM	LES (SGS)	2-phase	Piston	N/A	55	IH
15	Harbin Engineering University (Zhang et al., 2018)	SPH-H	P-NSL	FEM-SPH	—	1-phase	Piston	N/A	7	IH
16	Manchester Metropolitan University (Lin et al., 2019)	FNPF-MMU	P	FVM	—	1-phase	Dirichlet	N/A	40	IH
17	Manchester Metropolitan University (Chen et al., 2019)	openFOAM-MMU	NSL	FVM	—	2-phase	Dirichlet	N/A	147	OS
18	Korea Research Institute of Ships and Ocean Engineering (Ha et al., 2019)	STAR-CCM-KRISO	NSL	FVM	—	2-phase	Dirichlet	N/A	110	C
19	Technical University of Denmark (Engsig-Karup et al., 2016)	FNPF-SEM	P	SEM	—	1-phase	Relaxation	N/A	N/A	IH
20	Hohai University (Lin et al., 2016)	NEWTANK	NST	FDM	LES	2-phase	Piston	N/A	22	IH

Note: P, potential; NSL, NS-Laminar; NST, NS-Turbulent; IH, in-house; OS, open source; C, commercial; WC, weak coupling; L_{NS}, length of the Navier–Stokes subdomain before the cylinder in the case of weak coupling; $D/\Delta x$, cells dividing the cylinder diameter, where D is the diameter of the cylinder and Δx is the minimum horizontal cell size reported by the participants.

Table 2 Details about the participating institutes and numerical codes employed for simulation

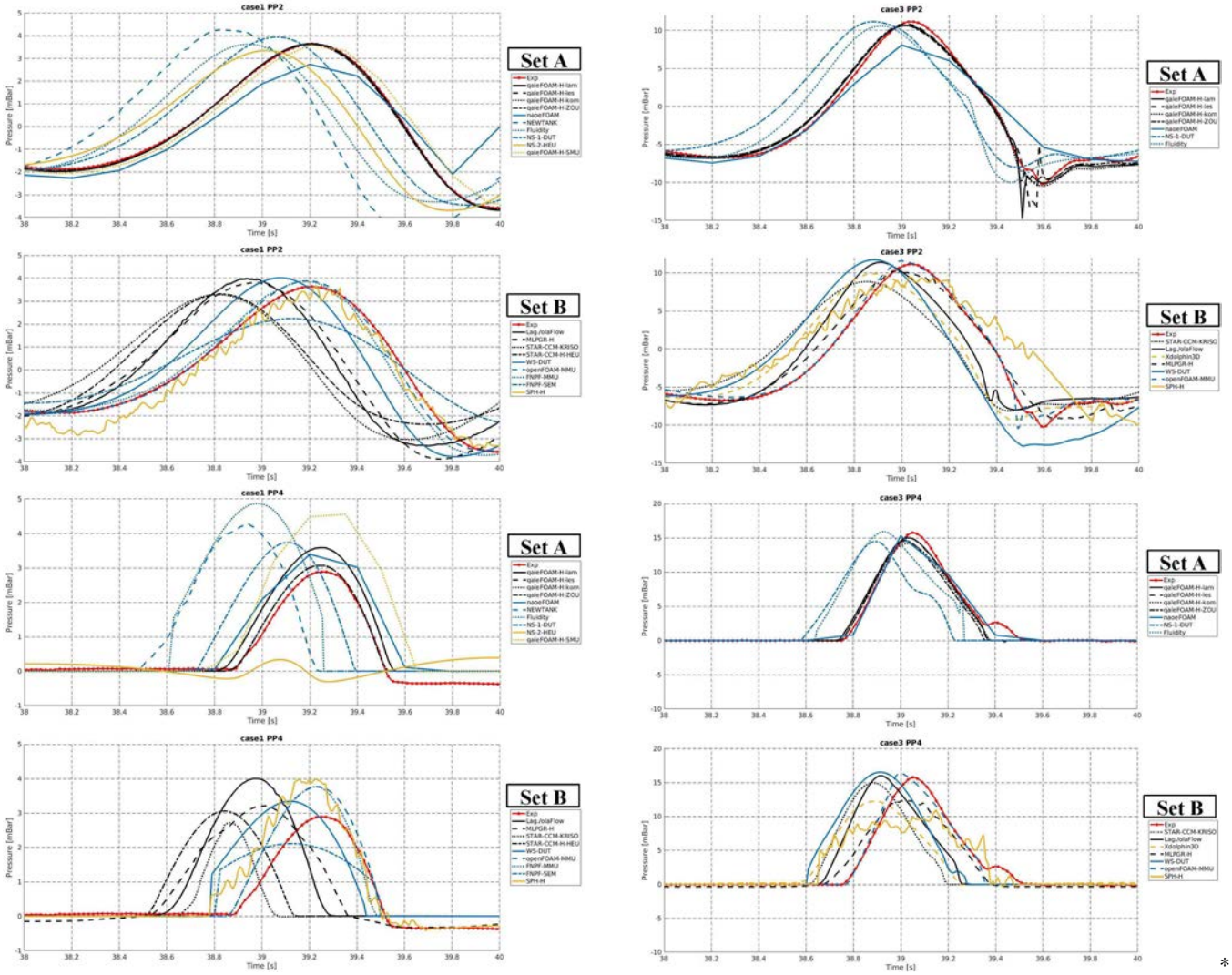

Fig. 4 Comparison of time series of dynamic pressure $p(t)$ signals recorded on the surface of the cylinder at probes located below (PP2: $z = -0.185$ m) and above the SWL (PP4: $z = +0.015$ m)

It is worth mentioning that, owing to the broad-banded nature of the target spectrum, there exists an overlap between the main energy band and the superharmonics (Sriram et al., 2015), which is visible in the experimental spectra at $f \gtrsim 0.75$ Hz.

Notice that the numerical capturing of this overlap is particularly challenging, because none of the solvers has been able to capture the nonlinear wave–wave interactions accurately. It may be concluded from Figs. 2 and 3 that the fidelity of replicating the focusing event is comparable across the various models. Although a majority of the solvers use either the full Navier–Stokes equations or hybrid modeling, neither modeling strategy shows any distinctive advantage in replicating the focusing event. It is interesting to note that the pure fully nonlinear potential theory (FNPT)-based "WS-DUT" model (set B) achieves excellent phase agreement but tends to overpredict the surface elevation, especially for case 3, as normally noticed in FNPT.

Accuracy in Capturing Pressure

The ability of the different solvers to replicate the focused wave pressure onto the structure is assessed here by comparing the time variation of dynamic pressure recorded on the submerged and exposed surfaces of the cylinder (see Fig. 4).

The evaluation is made for the probes PP2 and PP4, which are placed at $z = -0.185$ m and $z = +0.015$ m, respectively, from the still water level (SWL) and oriented at 0°—that is, facing wave attack. Given that PP2 lies at the stagnation point, the dynamic pressure variation is expected to resemble the incident wave elevation (at WP5). Accordingly, the simulated pressure histories from different solvers also exhibit the same trends as previously observed for WP5 in Figs. 2 and 3. That is, the simulations show an overall good agreement against experiments with a greater phase deviation being observed for the smaller wave in comparison to the larger wave. In the case of the "air probe" PP4, the intermittent loading event is correctly reproduced by a majority of the solvers for the steeper wave. However, a significant discrepancy exists in the simulated peak pressure values as well as loading duration for the smaller wave. Given that phase shift is not a major concern, the fact that the different solvers agree well in predicting the loading induced by the steeper wave is, in fact, promising from the designer's perspective. However, it is worth noting that the uncertainty in numerically predicting the loading induced by the smaller wave is much greater in comparison to that induced by the steeper wave.

Quantification of Relative Errors

The qualitative assessment shows the trend that provides an overall understanding of the variations encountered with different solvers. However, one cannot infer any conclusions from the

S/N	Code name	Processor model	OpenMP, MPI, GPU, Serial	No. of CPUs	Processor clock speed (GHz)	System RAM (GB)	Wall-clock run time (hrs)	System run time (hrs)
1	IITM MLPGR-H	Intel® Xeon® CPU E5-2650 v4	Serial/ OpenMP	8	2.2	34	11.9	—
2	qaleFOAM-H-lam	Intel® Xeon® CPU E5-2680 v4	OpenMP MPI	8	2.4	64	7.98	—
3	qaleFOAM-H-LES	Intel® Xeon® CPU E5-2680 v4	OpenMP MPI	16	2.4	64	42	—
4	qaleFOAM-H-kom	Intel® Xeon® CPU E5-2680 v4	OpenMP MPI	16	2.4	64	11.5	—
5	qaleFOAM-H-SMU	Intel® Xeon® E5 2690 v3	MPI	7	2.4	32	—	—
6	Xdolphin3D	Intel® Xeon® CPU E5-2660 v4	Serial/MPI	1	2.0	256	36	—
7	naoe-FOAM-SJTU	Intel® Core™ i7-7700	OpenMP	6	3.6	32	79.3	78.9
8	WS-DUT	Intel® Core™ i7-8700K	Serial	6	3.7	16	11.8	—
9	Fluidity	—	MPI	56	—	—	96	96
10	Lag./olaFlow	Intel® Xeon® Gold 6138	Serial/MPI	1/72	2.0	64	20 + 35	55
11	NS-1-DUT	Intel® Core™ i7-9700K	MPI	8	3.6	32	6.2	6.2
12	qaleFOAM-H-ZOU	Intel® Xeon® CPU E5-2680 v4	OpenMP MPI	16	2.4	64	21	—
13	STAR CCM-H-HEU	Intel® Xeon® CPU E5-2080 v2	MPI	40	2.8	64	62	—
14	NS-2-HEU	Intel® Core™ i7-7700HQ CPU	Serial	4	2.8	16	71.3	—
15	SPH-H	Intel® i7	OpenMP	16	3.3	128	—	4.44
16	FNPF-MMU	Intel® Xeon® E5-2600	MPI	16	1.7	64	10.23	10.21
17	openFOAM-MMU	Intel® Xeon® E5-2600	MPI	96	1.7	64	31.16	31.09
18	STAR-CCM-KRISO	Intel® Xeon® CPU E5-2640 v4	MPI	300	2.4	192	—	~6
19	FNPF-SEM	Intel® Xeon® 2660v3	Serial	6	2.6	16	96	—
20	NEWTANK	Intel® Xeon® CPU E5-2650	OpenMP	2	2.3	64	96	96

Table 3 Computational aspects of the different solvers

qualitative assessment, as only two wave probe and two pressure probe readings have been analyzed. Hence, the relative errors in physical quantities computed through the different solvers for four pressure probes and three wave probes near the cylinder are analyzed and presented here in terms of quartiles. The box plots for relative error in peak values of pressure $((p_{\max}^{\text{num}} - p_{\max}^{\text{exp}})/p_{\max}^{\text{exp}})$ and surface elevation $((\eta_{\max}^{\text{num}} - \eta_{\max}^{\text{exp}})/\eta_{\max}^{\text{exp}})$, recorded at various probe locations, are shown in Fig. 5. Here, quartiles for NSL and NST models are also reported separately to gain further insight into the capabilities of NS solvers, which have been used in $\sim 90\%$ of the studies (see Table 3). If one observes the quartiles of relative error in pressure, it can be seen that all solvers estimate the wave-induced dynamic pressure below the SWL at the stagnation point (PP2) within an error range of -25% to $+10\%$. For the steep wave (case 3), the tendency of the methods to underpredict the dynamic pressure increases slightly as the median error shifts from $\sim 0\%$ for the smaller wave to -5% for the steeper wave.

With regard to PP4, which is 0.015 m above the SWL and thus experiences intermittent loading, the quartiles indicate that the underprediction in the pressure peak is restricted to -10% within the interquartile range for the steep wave (case 3). However, the intermittent pressure peak gets largely overpredicted for the smaller wave, such that the median error is almost $+20\%$. Although small waves may not be deemed significant from a structural survivability perspective, the error quartiles indicate that the simulation of intermittent loading induced by small waves is indeed computationally challenging. The probes PP6 and PP8 are submerged at $z = -0.085$ m from the SWL but are offset by 20° and 180° from the wave attack. Thus, PP6 lies between the stagnation and separation points, whereas PP8 lies adjacent to the cylinder wake. The quartile plots in Fig. 5 indicate that at least 50% of the solvers (interquartile range) are able to predict the dynamic pressure peak at PP6 within an error range of 0% to 10% for both cases 1 and 3. Strictly speaking, in terms of the size of interquartile range, this is more or less the same range of uncertainty as previously observed for PP2 from Fig. 5. This should not come as a surprise because PP6 lies closer to the stagnation point, and thus static pressure variations caused by boundary layer separa-

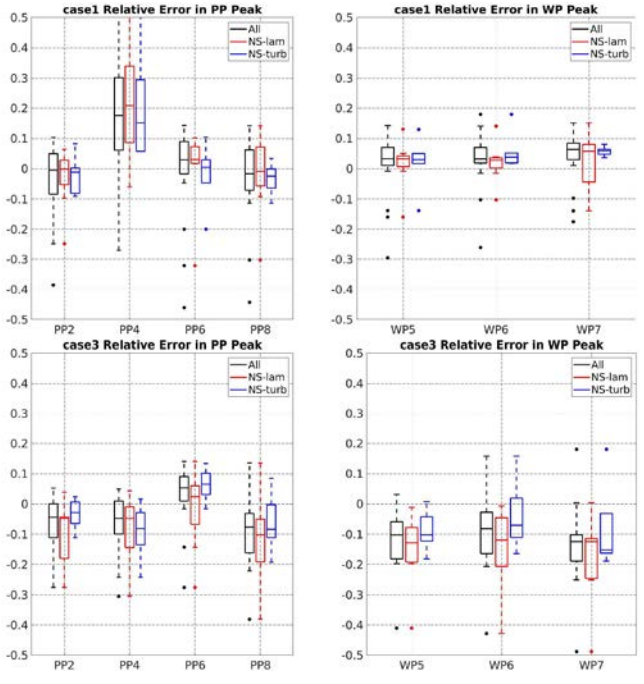

Fig. 5 Quartile-based representation of the relative error in peak values of pressure and surface elevation recorded at different probe locations and compared for different groups of methods

tion (which occur close to 90°) are negligible at 20°. Furthermore, this error behavior is seen to be independent of the wave steepness. Nonetheless, the wave steepness is seen to indeed influence the relative error at PP8, where the median of the solvers tends to correctly predict the dynamic pressure peak in the wake for the smaller wave but underpredict the peak for the steep wave. It is also worth noting that the overall relative error range is larger for the steeper wave at PP8. This may be related to stronger wake separation and turbulence effects induced for the steeper wave that lead to an increase in the median error as well as interquartile error range for numerical predictions. Overall, the acceptable median error is ±5%, with maximum and minimum acceptable ranges as ±10%. There are few solvers that show extreme values (dots in Fig. 5); those are not acceptable. If one compares the overall performance of all studies against that of the NS solvers, it can be seen that the joint performance is dictated by the relative fidelity of the NSL and NST solvers, as the median error of all studies is seen to always lie between the median errors of the NSL and NST studies. This is to be expected because the NS solvers constitute almost 90% of the submitted results. It is also interesting to note that the inclusion of turbulence modeling invariably results in an improvement in accuracy (shrinking of the interquartile range) in all cases, especially for the subsurface hydrodynamic loading induced by the steeper wave at the stagnation point (PP2) and in its vicinity (PP6).

The quartiles of relative error in the peak value of free-surface elevation measured at WP5–WP7 have also been reported on the right side of Fig. 5. It can be appreciated that all submitted solvers captured the focused peak accurately, with the median error restricted to at most + 5% for the smaller wave at WP5 and WP6. Furthermore, the inclusion of turbulence modeling is seen to improve the surface elevation prediction after the cylinder (WP7), especially for the smaller wave. However, for the steeper wave, there is a tendency for the simulations to underpredict the elevation of the focused peak as the median error is seen to be approximately −10% for all the three probes. Furthermore, the inclusion of turbulence modeling is not seen to have any significant impact in improving the prediction of the steeper focused peak as the interquartile range as well as the median error remains more or less the same across WP5–WP7. This tendency to underpredict the focused peak may be closely linked to a corresponding underprediction of the superharmonic spectral energy content, as evidenced from Fig. 3 and will be discussed later. The latter may, in turn, be linked to the limitations of the computational mesh in capturing the shorter, higher harmonic waves that are generated through nonlinear wave-wave interactions during the focusing process (Sriram et al., 2015). The wave-wave interactions are particularly manifested in the constant steepness approach wherein the steepness is constant throughout the spectral components.

To obtain greater physical insight into the processes of focused wave generation and its interaction with the cylinder and how well these processes were reproduced in the simulations, the relative energy error $((\sum S(f)^{\text{num}} - \sum S(f)^{\text{exp}})/\sum S(f)^{\text{exp}})$ quartiles have been represented over two frequency bands: (a) the primary band containing the focused wave ($f \in [0.34\colon 1.02$ Hz]) and (b) the sub- ($0 < f < 0.34$ Hz) and superharmonics ($1.02 < f < 2.04$ Hz) that fall outside the main band. The box plots quantifying relative error in spectral energy content ($S(f)$) corresponding to pressure and surface elevation recorded at various probe locations are shown in Fig. 6 for cases 1 and 3.

Referring to Fig. 6, the spectral energy error, corresponding to the pressure signals, has been depicted for the stagnation point (PP2), the separation point (PP7), and the wake (PP8). Broadly speaking, the dynamic pressure corresponding to the main frequency band has been captured more accurately for the steeper wave (case 3). The greater spread in spectral energy error for case 1 may be attributed to a general limitation of the numerical models not being able to capture the low-amplitude variations induced in subsurface pressure by the smaller waves. This statement is corroborated by the significantly larger error spread in the sub- and superharmonic ranges at PP2 for case 1 (in comparison to case 3),

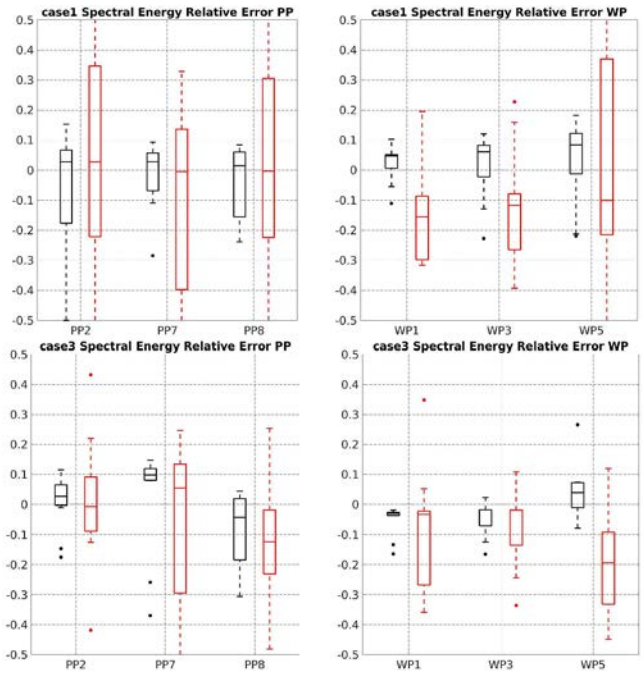

Fig. 6 Quartile-based representation of the relative error in spectral energy content within the primary band (black color) as well as sub- and superharmonics (red color) corresponding to $\eta(t)$ and $p(t)$ series recorded at different probe locations

which hints at a general difficulty in capturing small-amplitude, high-frequency waves in the simulations. Interestingly, the relative energy error trend is slightly different in the wake region (PP8). The relative error spread in capturing the wake pressure within the main frequency range is comparable for both waves, with the models exhibiting a general tendency to underpredict the wake pressure. However, outside the main range, the median error is $\sim 0\%$ for case 1. This means that the solvers are equally likely to underpredict or overpredict the wake pressure in the sub- and superharmonic ranges for the smaller wave. By contrast, the quartiles indicate that almost 75% of the solvers would underpredict the sub- and superharmonics' induced pressure within the wake for the larger wave.

Finally, the relative energy error quartiles for the surface elevation signals are briefly discussed here. A clear-cut trend of the surface elevation error emerges within the main frequency band from Fig. 6. Irrespective of the focused wave design, the error is observed to show an increasing trend (the quartiles spread wider) as one moves from WP1 (close to the wavemaker) to WP3 ($\sim$14 m from the wavemaker) and finally to WP5 (in front of the cylinder) along the numerical wave tank. This is indicative of a general accumulation of numerical error in the simulations, but it also suggests that significant effort was put in by the participants toward getting a near-exact match against experiments for the $\eta(t)$ signal at WP1. Obviously, this is to be expected because the free-surface elevation history at WP1 represents the "incident wave packets" whose fidelity is crucial to the accuracy of the entire simulation. It is also observed from Fig. 6 that the relative energy error for the surface elevation is significantly greater outside the main frequency range. Although this is true for both waves, the quartiles spread wider for case 1, which yet again highlights an inherent limitation of the computational solvers to sufficiently capture the sub- (insufficient cells/particles to resolve wave height) and superharmonics (insufficient cells/particles to resolve wavelength) of the smaller wave. Furthermore, the quartiles indicate a general increase in relative spectral energy error outside the main band as one moves from WP1 to WP5, with the energy getting underpredicted in case of the steep wave. This, yet again, is attributable to accumulation of numerical error and/or numerical damping of the waves, especially after $\sim$25 m of propagation to reach WP5 close to the cylinder.

Comparison of CPU Effort

One may presume that the current advancement in computational power, hardware capacity, high-performance computing, and software architecture would lead to faster computation of nonlinear focused wave interactions with a fixed cylinder in a large domain. Somewhat contrary to this presumption, Table 3 indicates that the run time for a single simulation is more than a day in most of the codes, and these simulations have been carried out mostly using a workstation. In particular, most of the in-house codes are OpenMP or MPI paralleled. It is also worth noting from Table 3 that the hybrid methodologies are about $2\times$ faster in comparison to the full/conventional NS solvers and yet achieve a comparable level of accuracy. However, the simulation time for some NST (LES) computation using a hybrid method is still $\sim$2 days, which is significant. This shows that there still exists scope for improvement in solver capability to speed up the computations for large-scale industrial needs. However, a need to develop new methodology should be considered in these directions, such as matrix-free algorithms and dynamic programming, rather than relying on augmentation in high-performance computing architecture.

CONCLUSIONS

The paper discusses the comparative study of 20 different solvers as part of the experimental data presented at ISOPE-2020. Based on the analysis carried out in the paper, the following observations are provided, which are applicable to a given solver for focused wave–monopile interactions:

1. Near to the wavemaker (< 5 m), the performance of all the solvers is promising. Thus, the acceptable relative error for a solver in capturing the primary energy content should be $\leq 5\%$, irrespective of the method of wave-generation adopted.
2. Far away from the wavemaker (say, $\sim$25 m—i.e., $10\times$ the average wavelength), the relative error increases to $\sim$10% in primary energy content. However, higher deviations ($\sim$50%) are expected for sub- and superharmonic components manifested through nonlinear wave-wave interactions during propagation.
3. The error, in general, will be higher for a small-amplitude case compared with a steep case in focusing waves. However, to ensure sufficient accuracy of the simulation, the error should be restricted within the limits specified in guidelines 1 and 2 in terms of the energy content. In the present comparative study, all the solvers captured the focused wave peaks within a median relative error of approximately $+5\%$ for the smaller wave and approximately -10% for the steep wave, which is promising.
4. The pressure peaks induced by the focusing event should be captured within an error range of $\pm 5\%$. All the solvers in the present study captured the pressure peaks with a median relative error of less than $\pm 4\%$.
5. The deviations in phase shift may be attributed to the deviations in sub- and superharmonics. However, the performance of a given solver in context to industrial applications need not be judged based on phase shift, as the design focus would be on accurately estimating the values of peak loads/pressures.
6. The "pure" FNPT simulations tend to overpredict the surface elevation as well as the wave-induced pressure at the point of focusing but achieve a near-exact agreement in phase with the experiments.
7. The inclusion of a turbulence model invariably improves accuracy, especially in the prediction of subsurface pressure induced by steep waves in the vicinity of the forward stagnation point.
8. Furthermore, the methods of generation using piston, relaxation zone, and Dirichlet type are all within an acceptable limit, and one is not superior to others.

Thus, based on the results obtained from 20 different solvers, the above observations have been noticed, which may be followed. It should be noted that the experimental error/uncertainty should also be taken into consideration during validation (see Sriram et al., 2021). The inclusion of the experimental uncertainty would make the above guidelines less stringent; however, it is always better to be conservative (and maintain a reduced error margin) when adopting the said guidelines in practice. In the case of deviations, the solver would have to be improved for wave interactions with fixed structure. It is also worth mentioning that the above guidelines hold irrespective of regular or random waves, as the tested conditions are for small-amplitude and steep focused waves generated using a constant steepness spectrum. Nevertheless, experiments involving regular and steep-breaking-focused waves interacting with a fixed as well as a moving cylinder may also be considered within the scope for future comparative studies. Furthermore, the state of the art in modeling large domain problems for transient waves appears to be based on hybrid numerical modeling using weakly coupled algorithms (or one-way coupling); this strategy was adopted by most of the participants. For

this coupling, the length of the domain used by many authors (i.e., from inlet to cylinder location) varies between 2 m and 4 m. However, it is noteworthy that strongly coupled algorithms have not been adopted by any of the researchers in this comparative study probably because the same are preferred only for non-transient periodic waves. A strong coupling between constituent solvers should be adopted in the future (even though challenging to implement) for reflection-dominant cases. The present comparative study is carried out for small-scale experimental studies; the future comparative direction should also be based on a large-scale study including air entrainment and compressibility effects.

ACKNOWLEDGEMENTS

The first author thanks the Alexander Von Humboldt Foundations and German Academic Exchange Service (DAAD), DST-UKIERI (DST-UKIERI-2016-17-0029 and DST/INT/UK/P-122/2016) for the experiments and numerical model developments of MLPG and qaleFOAM.

REFERENCES

Agarwal, S, Saincher, S, et al. (2021). "A Comparative Study on the Nonlinear Interaction Between a Focusing Wave and Cylinder Using State-of-the-art Solvers, Part B," *Int J Offshore Polar Eng,* ISOPE, 31(1), 11–18. https://doi.org/10.17736/ijope.2021.jc832.

Agarwal, S, Sriram, V, Yan, S, and Murali, K (2021). "Improvements in MLPG Formulation for 3D Wave-fixed Structure Interaction," *Comput Fluids,* 218, 104286. https://doi.org/10.1016/j.compfluid.2020.104826.

Ai, C, Jin, S, and Lv, B (2011). "A New Fully Non-hydrostatic 3D Free Surface Flow Model for Water Wave Motions," *Int J Numer Methods Fluids*, 66(11), 1354–1370. https://doi.org/10.1002/fld.2317.

Ai, C, Ma, Y, Yuan, C, and Dong, G (2019). "Development and Assessment of Semi-implicit Non-hydrostatic Models for Surface Water Waves," *Ocean Modell*, 144, 1–15. https://doi.org/10.1016/j.ocemod.2019.101489.

Buldakov, E, Higuera, P, and Stagonas, D (2019). "Numerical Models for Evolution of Extreme Wave Groups," *Appl Ocean Res*, 89, 128–140. https://doi.org/10.1016/j.apor.2019.05.013.

Chen, H, et al. (2019). "Application of an Overset Mesh Based Numerical Wave Tank for Modelling Realistic Free-surface Hydrodynamic Problems," *Ocean Eng*, 176, 97–117. https://doi.org/10.1016/j.oceaneng.2019.02.001.

Clément, AH (1999). "Benchmark Test Cases For Numerical Wave Absorption: 1st Workshop of ISOPE Numerical Wave Tank Group, Montréal, May 1998," *Proc 9th Int Offshore Polar Eng Conf*, Brest, France, ISOPE, 3, 266–289.

Engsig-Karup, AP, Eskilsson, C, and Bigoni, D (2016). "A Stabilised Nodal Spectral Element Method for Fully Nonlinear Water Waves," *J Comput Phys*, 318, 1–21. https://doi.org/10.1016/j.jcp.2016.04.060.

Gong, J, Yan, S, Ma, QW, and Li, Y (2020). "Added Resistance and Seakeeping Performance of Trimarans in Oblique Waves," *Ocean Eng*, 216, 107721. https://doi.org/10.1016/j.oceaneng.2020.107721.

Ha, YJ, Nam, BW, Kim, KH, and Hong, SY (2019). "CFD Simulations of Wave Impact Loads on a Truncated Circular Cylinder by Breaking Waves," *Int J Offshore Polar Eng*, ISOPE, 29(3), 306–314. https://doi.org/10.17736/ijope.2019.ak33.

Higuera, P (2020). "Enhancing Active Wave Absorption in RANS Models," *Appl Ocean Res*, 94, 102000. https://doi.org/10.1016/j.apor.2019.102000.

Li, Q, Wang, J, Yan, S, Gong, J, and Ma, QW (2018). "A Zonal Hybrid Approach Coupling FNPT with OpenFOAM for Modelling Wave-structure Interactions with Action of Current," *Ocean Syst Eng*, 8(4), 381–407. https://doi.org/10.12989/ose.2018.8.4.381.

Liao, KP, Duan, WY, et al. (2017). "Numerical Analysis of Wave Impact Loads on Semi-submersible Platform," *Proc 36th Int Conf Ocean Offshore Arct Eng*, Trondheim, Norway, ASME, 1, V001T01A084. https://doi.org/10.1115/OMAE2017-62464.

Liao, KP, and Hu, CH (2013). "A Coupled FDM-FEM Method for Free Surface Flow Interaction with Thin Elastic Plate," *J Mar Sci Technol*, 18(1), 1–11. https://doi.org/10.1007/s00773-012-0191-0.

Lin, P, Cheng, L, and Liu, D (2016). "A Two-phase Flow Model for Wave–structure Interaction Using a Virtual Boundary Force Method," *Comput Fluids*, 129, 101–110. https:// doi.org/10.1016/j.compfluid.2016.02.007.

Lin, Z, et al. (2019). "Development of a 3D Fully Nonlinear Potential Flow Wave Tank in Framework of OpenFOAM," *Proc 38th Int Conf Ocean Offshore Arct Eng*, Glasgow, UK, ASME, 9, OMAE2019-96098.

Loysel, T, et al. (2012). "Results of the First Sloshing Model Test Benchmark," *Proc 22nd Int Offshore Polar Eng Conf*, Rhodes, Greece, ISOPE, 3, 398–408.

Ma, Y, Yuan, C, Ai, C, and Dong, G (2019). "Comparison between a Non-hydrostatic Model and OpenFOAM for 2D Wave-structure Interactions," *Ocean Eng*, 183, 419–425. https://doi.org/10.1016/j.oceaneng.2019.05.002.

Ransley, E, et al. (2019). "A Blind Comparative Study of Focused Wave Interactions with a Fixed FPSO-like Structure (CCP-WSI Blind Test Series 1)," *Int J Offshore Polar Eng*, ISOPE, 29(2), 113–127. https://doi.org/10.17736/ijope.2019.jc748.

Ransley, E, et al. (2020). "A Blind Comparative Study of Focused Wave Interactions with Floating Structures (CCP-WSI Blind Test Series 3)," *Int J Offshore Polar Eng*, ISOPE, 30(1), 1–10. https://doi.org/10.17736/ijope.2020.jc774.

Shen, Z, and Wan, D (2016). "An Irregular Wave Generating Approach Based on naoe-FOAM-SJTU Solver," *China Ocean Eng*, 30(2), 177–192. https://doi.org/10.1007/s13344-016-0010-1.

Sriram, V, Agarwal, S, and Schlurmann, T (2021). "Laboratory Study on Steep Wave Interactions with Fixed and Moving Cylinder," *Int J Offshore Polar Eng*, ISOPE, 31(1), 19–26. https://doi.org/10.17736/ijope.2021.jc808.

Sriram, V, Schlurmann, T, and Schimmels, S (2015). "Focused Wave Evolution Using Linear and Second Order Wavemaker Theory," *Appl Ocean Res*, 53, 279–296. https://doi.org/10.1016/j.apor.2015.09.007.

Tanizawa, K, and Clément, AH (2000). "Report of the 2nd Workshop of ISOPE Numerical Wave Tank Group: Benchmark Test Cases of Radiation Problem, (Brest, May 1999)," *Proc 10th Int Offshore Polar Eng Conf*, Seattle, WA, USA, ISOPE, ISOPE-I-00-242.

Wang, Q, Zhai, Z, Liao, K, Ma, Q, and Shao, Y (2020). "Study on Interaction of Steep Focused Waves with Fixed Cylinder Based on CFD Method," *Proc 30th Int Ocean Polar Eng Conf*, Shanghai, China, ISOPE, 3, 2293–2298.

Xie, Z, Lu, L, et al. (2017). "Numerical Simulation of Three-dimensional Breaking Waves and Its Interaction with a Vertical Circular Cylinder," *J Hydrodyn*, 29(5), 800–804. https://doi.org/10.1016/S1001-6058(16)60791-6.

Xie, Z, and Stoesser, T (2020). "A Three-dimensional Cartesian Cut-cell/volume-of-fluid Method for Two-phase Flows with Moving Bodies," *J Comput Phys*, 416, 109536. https://doi.org/10.1016/j.jcp.2020.109536.

Yan, S, Wang, J, Wang, J, Ma, Q, and Xie, Z (2020). "CCP-WSI Blind Test Using qaleFOAM with an Improved Passive Wave Absorber," *Int J Offshore Polar Eng*, ISOPE, 30(1), 43–52. https://doi.org/10.17736/ijope.2020.jc781.

Zhang, NB, et al. (2018). "A Hybrid Stabilization Technique for Simulating Water Wave-structure Interaction by Incompressible Smoothed Particle Hydrodynamics (ISPH) Method," *J Hydroenviron Res*, 18, 77–94. https://doi.org/10.1016/j.jher.2017.11.003.

Zhang, Y, and Teng, B (2019). "A Nonlinear Potential Flow Model for High-frequency Wave Loads and Ringing Response of Offshore Wind Turbines," *Proc 29th Int Ocean Polar Eng Conf*, Honolulu, HI, USA, ISOPE, 1, 304–311.

Zhang, Y, Teng, B, and Ning, DZ (2020). "Comparative Study on Interaction of Steep Focused Waves with a Fixed Cylinder by HOBEM," *Proc 30th Int Ocean Polar Eng Conf*, Shanghai, China, ISOPE, 3, 2228–2235.